ChemComm

COMMUNICATION

View Article Online
View Journal | View Issue

Cite this: *Chem. Commun.*, 2025, **61**, 11199

Received 14th April 2025,
Accepted 16th June 2025

DOI: 10.1039/d5cc02095f

rsc.li/chemcomm

High throughput screening of high entropy spinel electrolytes for multivalent batteries†

Mahesh J. Dheerasinghe,‡[a] Yi Gan,‡[b] Lin Wang,[a] Yufang He,[a] Zhengda He,[a] Gui-Liang Xu,[c] Yang Zhao *[b] and Bin Ouyang *[a]

High-entropy (HE) design emerged as a promising path for discovering multivalent superionic conductors. This work provides a computational exploration of the synthesizability of HE spinel-based electrolytes among the typical chemical space. Design principles have been established, while experimental synthesis has supported the stability rules predicted by computational data.

With the rapid advancement of electric vehicles, portable electronics, and mobile robotics, the demand for rechargeable batteries with higher energy density and improved safety continues to grow.[1] Electrolytes are key to enhancing long-term cycling stability by effectively suppressing the formation of lithium dendrites-a major safety concern.[2] To further improve energy storage capabilities, multivalent-ion batteries have gained attention as promising alternatives due to their potential for higher volumetric energy density. Unlike monovalent ions such as Li^+/Na^+/K^+, multivalent ions (*e.g.*, Mg^{2+}, Al^{3+}) carry multiple charges per ion, enabling greater energy storage potential.[3–5] Moreover, multivalent metals exhibit reduced tendency to form dendrites compared to lithium, contributing to enhanced safety and stability in multivalent systems.[6]

Despite substantial developments in multivalent electrode[7] materials, the relative deficiency of robust solid-state electrolytes presents a significant challenge to developing safer energy storage technologies. Materials with spinel structures are widely recognized for their potential in various rechargeable batteries applications.[8–12] The general chemical formula AM_2X_4 allows divalent cations to occupy the A site, which adopts tetrahedral coordination, while charge balance is maintained by cations at the octahedral M sites. The anion site, represented by X, can be occupied by oxygen, sulfur or halogens. In this work, we will focus primarily on oxide-based spinel due to their exceptional phase stability and electrochemical stability. Despite the advantages, spinel-based multivalent systems suffer from sluggish ion migration within the lattice.[13] This challenge might be mitigated through HE strategy, which boost ionic conductivity *via* compositional disorder[14] that creates overlapping site energies which promote the formation of ion-percolating networks. Moreover, the synthetic accessibility of such materials has the potential to be enhanced by entropy stabilization mechanism.[15]

In this work, we present a systematic high-throughput screening of potential spinel oxide-based HE electrolytes, with a focus on addressing the synthesis challenges of these materials. We computationally investigated the phase stability of AM_2O_4 HE spinel oxides, with Mg, Ca and Zn being the mobile ions at A site, while the M sites are contributed by 4 equal-molar species out of 14 cations that can reach charge balance. Phase diagrams have been analyzed across 381 compounds to reveal the thermodynamic stability principles for compositional design. Finally, experimental synthesis has been performed to support the viability of our theoretical predictions.

This study focused on spinel electrolytes based on Mg^{2+}, Zn^{2+}, and Ca^{2+}, where these three divalent cations occupy the tetrahedral sites within the spinel structures. Accordingly, all spinels were categorized as Mg-, Zn-, and Ca-based, respectively. The spinel structure with a single metal at the M site is used as a template to generate HE versions by substituting the octahedral sites (M) with four different metal cations, selected in equimolar concentrations from a pool of 14 redox inactive ions: Mg^{2+}, Zn^{2+}, Ca^{2+}, Al^{3+}, Ga^{3+}, In^{3+}, Sc^{3+}, Zr^{4+}, Hf^{4+}, Ti^{4+}, Sn^{4+}, Nb^{5+}, Ta^{5+}, and Sb^{5+}, while ensuring overall charge neutrality. As a result, 127 distinct HE compositions have been generated for each divalent metal in A site.

Subsequently, we performed a high-throughput phase diagram[16] calculations among the identified 381 HE spinels using Density function theory (DFT) to assess their stability. (see ESI† for computational methods) DFT simulations were employed to all three spinel categories, utilizing the ground states from materials

[a] *Department of Chemistry and Biochemistry, Florida State University, Tallahassee, FL, USA. E-mail: bouyang@fsu.edu*
[b] *Department of Mechanical and Materials Engineering, The University of Western Ontario, Canada*
[c] *Chemical Sciences and Engineering Division, Argonne National Laboratory, Lemont, IL, USA*

† Electronic supplementary information (ESI) available. See DOI: https://doi.org/10.1039/d5cc02095f

‡ These authors contributed equally to this work.

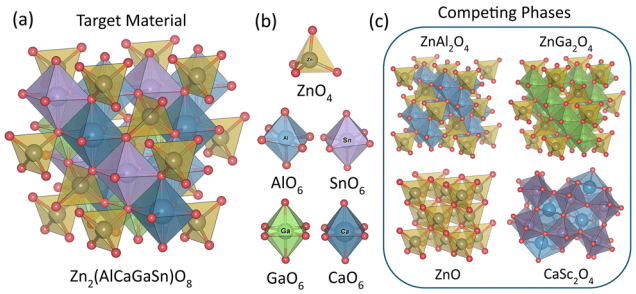

Fig. 1 (a) One example of HE Zn-spinel; (b) tetrahedral site and octahedral sites of metals, (c) competing phases of the selected material.

project database to construct phase diagrams.[16,17] One representative candidate, chosen as $Zn_2(AlCaGaSn)O_8$, is illustrated in Fig. 1 to clarify this process. In this material, Zn^{2+} stays in tetrahedral site, while four other metals will occupy octahedral sites. From phase diagram calculations, there are four competing phases-$ZnAl_2O_4$, $ZnGa_2O_4$, ZnO, and $CaSc_2O_4$ for the targeted composition, while the energy above the convex hull (E_{hull}) made from these four competing phases can serve as quantitative metric for evaluating the synthesizability. E_{hull}, defined as the decomposition energy of a target material into the ground state (*i.e.*, the convex hull) in the corresponding phase diagram, has been shown in various prior studies to possess remarkable capability in quantifying synthesizability,[5,18–21] and is therefore adopted in this work. A total of 26, 35, and 24 competing phases were identified for Mg-, Zn-, and Ca-based spinels, respectively. Fig. 2 presents the frequency distribution of these competing phases. As depicted, the most encountered competing phases for Mg-, Zn-, and Ca-based systems are MgO, ZnO, and $CaIn_2O_4$, respectively (see ESI† for competing phases).

As HE materials become increasingly stable at elevated temperatures due to configurational entropy contributions, the temperature at which the target phase becomes thermodynamically favored is defined as the entropy stabilization temperature ($T_{stabilized}$), calculated as: $T_{stabilized} = E_{hull}/S_{config}$ (refer to the ESI† for the $T_{stabilized}$ values).[15,21] Based on this analysis, 53 target phases exhibit entropy stabilization temperatures below 1473 K, which is set us a proxy for the upper temperature limit for classical solid-state reaction. The application of this filtering criterion yields 19, 26, and 8 stable phases from the Mg-, Zn-, and Ca-based spinels, respectively. This also suggests that spinel structures incorporating Zn^{2+} at the tetrahedral site demonstrate the greatest synthetic stability under ambient conditions, whereas Ca-based spinels appear to be least stable within the same temperature range.

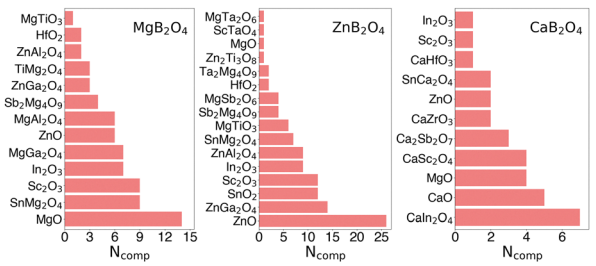

Fig. 2 Occurrence frequency of competing phases in Mg-, Zn- and Ca-based spinels.

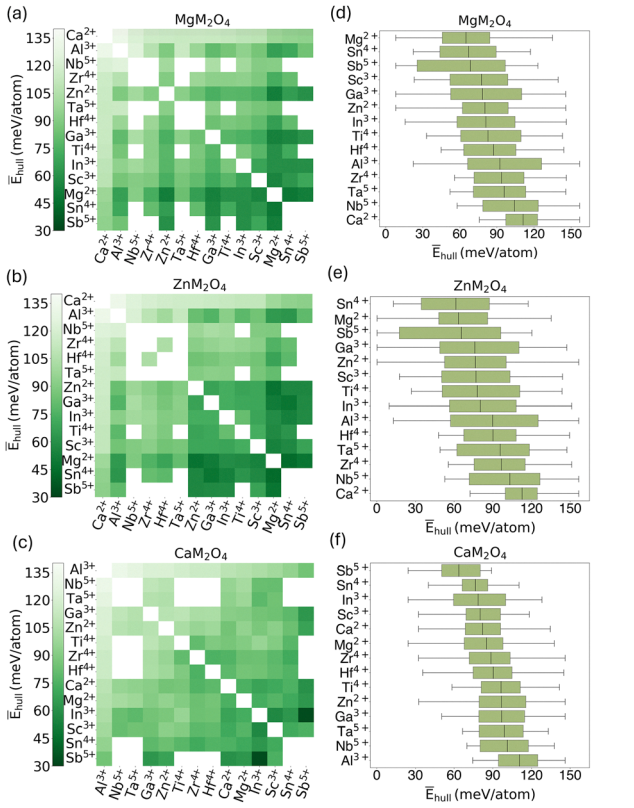

Fig. 3 Thermodynamic stability of HE spinels based on (a) and (d) Mg, (b) and (e) Zn, and (c) and (f) Ca as A-site cations. Subfigures (a)–(c) show heatmaps of the average energy above hull ($\bar{E}_{hull}$) in meV per atom for different cation pairs occupying the octahedral (M) sites; Subfigures (d)–(f) present box plots of E_{hull} distributions for individual cations.

To provide a better picture of the thermodynamic stability trends, heatmaps and boxplots derived from the calculated E_{hull} values are presented in Fig. 3(a–c) displays heatmaps representing the average E_{hull} values among all compositions that have the given pairs of metals. These plots reveal trends in cation compatibility, where darker regions indicate more stable cation pairings (lower E_{hull}), and lighter regions correspond to less stable combinations (higher E_{hull}). Such patterns provide insights into favorable elemental substitutions that help enhance the thermodynamic stability in HE spinel systems.[20–24] Meanwhile, Fig. 3(d–f) display box plots illustrating the distribution of E_{hull} values for individual cations occupying octahedral-sites in Mg-, Zn-, and Ca-based spinels. Cations with lower median E_{hull} values are associated with higher stability, while the width of the distribution reflects their sensitivity to the surrounding chemical environment. Narrow distributions indicate consistent stability across compositions, whereas broader ones suggest greater variability. It can be inferred from Fig. 3 that among the Mg- and Zn-based spinels, the most stabilizing elements in the octahedral sublattice include Mg^{2+}, Sn^{4+}, and Sb^{5+} whereas Ca^{2+} and Nb^{5+} appear to be the least favorable. In Ca-based spinels, however, the stability trend slightly diverges. Although Ca^{2+} contributes to instability when present in the octahedral sites of Mg- and Zn-based spinels, it exhibits moderate stability within its own species of Ca-based spinels. For these systems, Al^{3+} and Nb^{5+} turn out to be the least

stable elements, whereas Sb^{5+}, Sn^{4+}, and In^{3+} displayed strong stabilizing behavior.

To further understand the fundamental chemical handles for tuning the synthesizability of the HE spinels, we attempted several elemental descriptors, *e.g.*, electronegativity, ionic radii and oxidation number, and have identified that average electronegativity ($\bar{\chi}$) and the standard deviation of ionic radius (σr_{ion}) of octahedral-site elements correlate best with phase stability. In Mg- and Zn-based spinels, $\bar{\chi}$ shows a moderate negative linear correlation with E_{hull}, with Pearson correlation coefficients (r) of −0.552 and −0.619, respectively (Fig. 4a and b). However, this trend is absent in Ca-based spinels, where the correlation is negligible, (*e.g.*, r = 0.108, as shown in Fig. 4c). Meanwhile, the σr_{ion} exhibits a strong positive linear relationship with E_{hull} for Mg- and Zn-based spinels, with r values of 0.813 and 0.793, respectively (Fig. 4e and f). Once again, Ca-based spinels deviate from this behavior, showing minimal correlation (r = 0.020; Fig. 4f). The strength of the inverse relationship between σr_{ion} and thermodynamic stability also follows the trend Ca ≪ Zn < Mg, which inversely correlates with the ionic radii of the tetrahedral site cations (Ca^{2+}: 1.00 Å, Zn^{2+}: 0.60 Å, Mg^{2+}: 0.57 Å).

Even though stability of Ca-spinels is less correlated with $\bar{\chi}$ and σr_{ion}, there are much better correlations with standard deviation of electronegativity ($\sigma\chi$) and average ionic radius ($\bar{r}_{ion}$) instead. Particularly, the Pearson correlation with $\sigma\chi$ and $\bar{r}_{ion}$ are −0.437 and −0.634 respectively (Fig. 4d and h). These deviations in the Ca-based spinels may be attributed to the significantly larger ionic radius and lower electronegativities of Ca^{2+}, which likely disrupt structural compatibility within the spinel lattice. As a result, the major factor for stability will be whether the metal ions have closer (larger) ionic radii compared to Ca^{2+} and possess sufficiently varied electronegativities to be compatible with the Ca-spinel framework. (See ESI† for the relationship between X and r_{ion} of octahedral site elements.)

To further understand the chemical bonding origin of stability, crystal orbital Hamilton population (−COHP) analysis was performed on the Mg-, Zn-, and Ca-based spinel systems, each featuring identical M-site (octahedral) compositions.[25] As shown by Fig. 5, the analysis focuses on interactions at the tetrahedral sites across these systems. As can be observed from Fig. 5(a), (c) and (e), Mg–O bond shows mostly bonding states, indicated by only green (positive) –COHP values. As a contrast, the Zn–O bond shows moderate antibonding character, while the Ca–O bond exhibits predominantly antibonding states, *e.g.*, red (negative) –COHP values. Such distinct chemical bonding features highlight the instability of Ca-based spinels mainly arises from the unstable Ca–O bond. Fig. 5(b), (d) and (f) can further support this point, as the M–O bond are quite similar across all three systems. The observations from chemical bond analysis are also consistent with the statistic observation that Ca tends to destabilize in tetrahedron environment in compounds like spinel compared to Mg and Zn based compounds.[26]

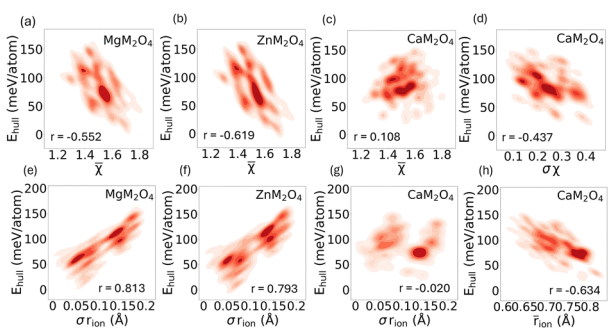

Fig. 4 Correlation analysis between E_{hull} and structural descriptors of octahedral-site elements in HE spinels. (a)–(c) Relationship between E_{hull} and $\bar{\chi}$. (e)–(g) Correlation between E_{hull} and σr_{ion} for Mg-, Zn-, and Ca-based spinels, respectively. (d) and (h) Illustrate the relationships between E_{hull} and the $\sigma\chi$, and between E_{hull} and $\bar{r}_{ion}$.

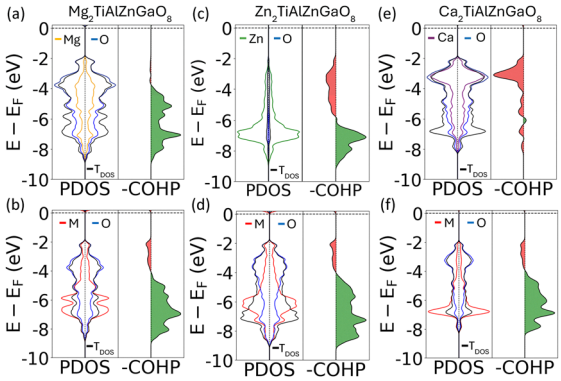

Fig. 5 Projected density of state (PDOS) and −COHP analyses for Mg-, Zn-, and Ca-based spinels with identical octahedral-site elements. Panels (a) and (c), and (e) correspond to Mg–O, Zn–O, and Ca–O bonding in the tetrahedral sites, respectively. Panels (b), (d), and (f) correspond to Ti–O, Al–O, Zn–O, and Ga–O (denoted as M) at octahedron sites.

To experimentally validate the computational predictions, six selected spinel structures, two each from the Mg-, Zn-, and Ca-based spinel groups are picked. The corresponding powder X-ray diffraction (XRD) patterns are presented in Fig. 6, with $ZnFe_2O_4$ (ICSD: PDF# 01-070-6393) used as a reference.[27] Notably, the samples $Mg_2(ZnMgSbIn)O_8$, $Mg_2(ZnMgSbGa)O_8$, $Zn_2(MgZnSbIn)O_8$, and $Zn_2(MgZnSbGa)O_8$ exhibit diffraction patterns consistent with the spinel phase, closely matching the reference material. In contrast, both Ca-based spinel samples are not synthesized successfully, as being indicated by the extra diffraction peaks in Fig. 6. The calculated E_{hull} values are provided together with each of the diffraction patterns. The synthesis outcome is consistent with the relative values of E_{hull}, while the two Mg-spinels and two Zn-spinels selected show much lower E_{hull} values, turn out to be phase pure. As a contrast, the two Ca-spinels, even though with lowest E_{hull} and third lowest E_{hull} values, still cannot be made phase pure.

To sum up, this study presents a high-throughput computational analysis, complemented by experimental validation of Mg-, Zn-, and Ca-based HE spinels as candidates for multivalent-ion electrolytes. Thermodynamic stability in HE spinels was found to correlate with the $\bar{\chi}$ and the σr_{ion} of octahedral site elements for Mg- and Zn-based spinels. However, Ca-based spinels show a divergent trend and unique correlation with $\sigma\chi$ and $\bar{r}_{ion}$. Based on the elemental study, the next challenge is to determine the optimal stoichiometry of the favorable metals, including Mg/Zn/Ca that maximizes ionic conductivity.[22,28]

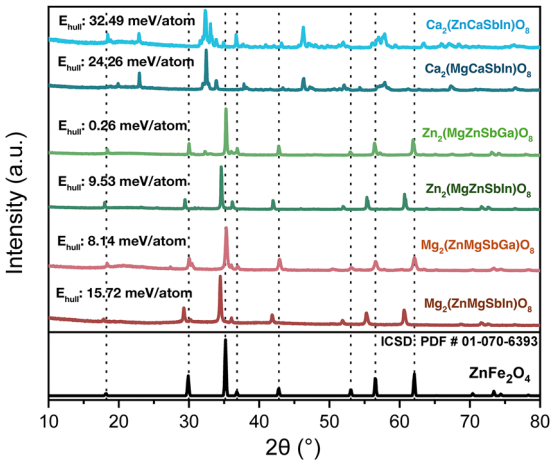

Fig. 6 Powder XRD patterns of synthesized HE spinel samples. Compositions are indicated in each panel of XRD patten.

This work was supported by startup funding from Florida State University. Computational resources were provided by the Advance Cyberinfrastructure Coordination Ecosystem: Services and Support (ACCESS) and the National Energy Research Scientific Computing Center (RCC) at Florida State University. Additional computation and data processing were supported by supercomputing recourses from the Department of Energy's Office of Energy Efficiency and Renewable Energy at the National Renewable Energy Laboratory. Research at Argonne National Laboratory was funded by the US Department of Energy (DOE), Vehicle Technologies Office. Support from S. Thompson and T. Duong of the US DOE's Office of Vehicle Technologies Program is gratefully acknowledged.

Conflicts of interest

There are no conflicts to declare.

Data availability

The data supporting this article have been included as part of the ESI.†

References

1 D. Zhang, Y. You, F. Wu, X. Cao, T.-Y. Lü, Y. Sun, Z.-Z. Zhu and S. Wu, Exploring the Relationship between Composition and Li-Ion Conductivity in the Amorphous Li–La–Zr–O System, *ACS Mater. Lett.*, 2024, **6**(5), 1849–1855.
2 Q. Liu, Z. Geng, C. Han, Y. Fu, S. Li, Y.-B. He, F. Kang and B. Li, Challenges and perspectives of garnet solid electrolytes for all solid-state lithium batteries, *J. Power Sources*, 2018, **389**, 120–134.
3 Q. Y. Zhao, G. Y. Yin, Y. F. Liu, R. R. Tang, X. W. Wu and X. X. Zeng, Recent advances in material chemistry for zinc enabled redox flow batteries, *Carbon Neutralization*, 2023, **2**(1), 90–114.
4 M. Al-Abbasi, Y. Zhao, H. He, H. Liu, H. Xia, T. Zhu, K. Wang, Z. Xu, H. Wang and W. Zhang, Challenges and protective strategies on zinc anode toward practical aqueous zinc-ion batteries, *Carbon Neutralization*, 2024, **3**(1), 108–141.
5 L. Wang, J. Wang and B. Ouyang, Computational Investigation of MAX as Intercalation Host for Rechargeable Aluminum-Ion Battery, *Adv. Energy Mater.*, 2023, **13**(46), 2302584.
6 Y. Tian, G. Zeng, A. Rutt, T. Shi, H. Kim, J. Wang, J. Koettgen, Y. Sun, B. Ouyang and T. Chen, Promises and challenges of next-generation "beyond Li-ion" batteries for electric vehicles and grid decarbonization, *Chem. Rev.*, 2020, **121**(3), 1623–1669.
7 Z. Rong, R. Malik, P. Canepa, G. Sai Gautam, M. Liu, A. Jain, K. Persson and G. Ceder, Materials design rules for multivalent ion mobility in intercalation structures, *Chem. Mater.*, 2015, **27**(17), 6016–6021.
8 Z. Cai, B. Ouyang, H.-M. Hau, T. Chen, R. Giovine, K. P. Koirala, L. Li, H. Ji, Y. Ha and Y. Sun, In situ formed partially disordered phases as earth-abundant Mn-rich cathode materials, *Nat. Energy*, 2024, **9**(1), 27–36.
9 M. Liu, A. Jain, Z. Rong, X. Qu, P. Canepa, R. Malik, G. Ceder and K. A. Persson, Evaluation of sulfur spinel compounds for multivalent battery cathode applications, *Energy Environ. Sci.*, 2016, **9**(10), 3201–3209.
10 Z. Cai, H. Ji, Y. Ha, J. Liu, D.-H. Kwon, Y. Zhang, A. Urban, E. E. Foley, R. Giovine and H. Kim, Realizing continuous cation order-to-disorder tuning in a class of high-energy spinel-type Li-ion cathodes, *Matter*, 2021, **4**(12), 3897–3916.
11 P. Canepa, S.-H. Bo, G. Sai Gautam, B. Key, W. D. Richards, T. Shi, Y. Tian, Y. Wang, J. Li and G. Ceder, High magnesium mobility in ternary spinel chalcogenides, *Nat. Commun.*, 2017, **8**(1), 1759.
12 L. Yin, B. J. Kwon, Y. Choi, C. J. Bartel, M. Yang, C. Liao, B. Key, G. Ceder and S. H. Lapidus, Operando X-ray diffraction studies of the Mg-ion migration mechanisms in spinel cathodes for rechargeable Mg-ion batteries, *J. Am. Chem. Soc.*, 2021, **143**(28), 10649–10658.
13 P. Canepa, G. Sai Gautam, D. C. Hannah, R. Malik, M. Liu, K. G. Gallagher, K. A. Persson and G. Ceder, Odyssey of multivalent cathode materials: open questions and future challenges, *Chem. Rev.*, 2017, **117**(5), 4287–4341.
14 Y. Zeng, B. Ouyang, J. Liu, Y.-W. Byeon, Z. Cai, L. J. Miara, Y. Wang and G. Ceder, High-entropy mechanism to boost ionic conductivity, *Science*, 2022, **378**(6626), 1320–1324.
15 B. Ouyang and Y. Zeng, The rise of high-entropy battery materials, *Nat. Commun.*, 2024, **15**(1), 973.
16 T.-L. Pham, L. Wang and B. Ouyang, Design principles for anode stable solid-state electrolytes, *J. Mater. Chem. A*, 2024, **12**(31), 19979–19987.
17 S. P. Ong, W. D. Richards, A. Jain, G. Hautier, M. Kocher, S. Cholia, D. Gunter, V. L. Chevrier, K. A. Persson and G. Ceder, Python Materials Genomics (pymatgen): A robust, open-source python library for materials analysis, *Comput. Mater. Sci.*, 2013, **68**, 314–319.
18 S. P. Ong, L. Wang, B. Kang and G. Ceder, Li− Fe− P− O2 phase diagram from first principles calculations, *Chem. Mater.*, 2008, **20**(5), 1798–1807.
19 W. Sun, S. T. Dacek, S. P. Ong, G. Hautier, A. Jain, W. D. Richards, A. C. Gamst, K. A. Persson and G. Ceder, The thermodynamic scale of inorganic crystalline metastability, *Sci. Adv.*, 2016, **2**(11), e1600225.
20 B. Ouyang, J. Wang, T. He, C. J. Bartel, H. Huo, Y. Wang, V. Lacivita, H. Kim and G. Ceder, Synthetic accessibility and stability rules of NASICONs, *Nat. Commun.*, 2021, **12**(1), 5752.
21 L. Wang, N. Sunariwal, Y. He, D.-H. Kim, D.-H. Yeon, Y. Zeng, J. Cabana and B. Ouyang, Elemental Stability Rules for High Entropy Disordered Rocksalt Type Li-Ion Battery Positive Electrodes, *Adv. Energy Mater.*, 2025, 2404982.
22 Y. Chen, Z. Lun, X. Zhao, K. P. Koirala, L. Li, Y. Sun, C. A. O'Keefe, X. Yang, Z. Cai and C. Wang, Unlocking Li superionic conductivity in face-centred cubic oxides via face-sharing configurations, *Nat. Mater.*, 2024, **23**(4), 535–542.
23 Z. Lun, B. Ouyang, D.-H. Kwon, Y. Ha, E. E. Foley, T.-Y. Huang, Z. Cai, H. Kim, M. Balasubramanian and Y. Sun, Cation-disordered rocksalt-type high-entropy cathodes for Li-ion batteries, *Nat. Mater.*, 2021, **20**(2), 214–221.
24 L. Wang, Z. He and B. Ouyang, Data driven design of compositionally complex energy materials, *Comput. Mater. Sci.*, 2023, **230**, 112513.
25 P. C. Müller, C. Ertural, J. Hempelmann and R. Dronskowski, Crystal orbital bond index: Covalent bond orders in solids, *J. Phys. Chem. C*, 2021, **125**(14), 7959–7970.
26 D. Waroquiers, X. Gonze, G.-M. Rignanese, C. Welker-Nieuwoudt, F. Rosowski, M. Gobel, S. Schenk, P. Degelmann, R. André and R. Glaum, Statistical analysis of coordination environments in oxides, *Chem. Mater.*, 2017, **29**(19), 8346–8360.
27 M. Bini, M. Ambrosetti and D. Spada, ZnFe2O4, a green and high-capacity anode material for lithium-ion batteries: A review, *Appl. Sci.*, 2021, **11**(24), 11713.
28 H. Ji, J. Wu, Z. Cai, J. Liu, D.-H. Kwon, H. Kim, A. Urban, J. K. Papp, E. Foley and Y. Tian, Ultrahigh power and energy density in partially ordered lithium-ion cathode materials, *Nat. Energy*, 2020, **5**(3), 213–221.

